

Three-dimensionally (3D) printing of propolis incorporated sodium alginate scaffolds for wound treatment

Muhammet UZUN¹ and Cem ÜSTÜNDAĞ²

¹Marmara University - Goztepe Campus

²Yildiz Technical University

April 28, 2020

Abstract

3D printing can be of great use, particularly the production of personal medical products and devices such as scaffolds. In this study, the main aim is to develop propolis (Ps) containing wound dressings by making use of 3D printing technology. Different combinations and structures of propolis (Ps) incorporated sodium alginate (SA) scaffolds are developed. The morphological studies show that the porosity of developed scaffolds was optimized when 20% (v/v) of Ps was added in the solution. The pore sizes decreased by increasing Ps concentration up to a certain level due to its adhesive properties. The mechanical, swelling-degradation (weight loss) behaviors and Ps release kinetics were highlighted for the scaffold stability. The antimicrobial assay was employed to test and screen antimicrobial behaviour of Ps against *Escherichia coli* and *Staphylococcus aureus* strains. The results show that the Ps added scaffolds have an excellent antibacterial activity because of Ps's compounds. The in-vitro cytotoxicity test was also applied on the scaffold by using the extract method on the human dermal fibroblasts (HFFF2) cell line. It is clearly found that the control SA and Ps added SA are non-toxic. The 3D printed SA-Ps scaffolds are very effective structures for wound dressing applications with unique properties.

1. INTRODUCTION

Additive manufacturing (AM) or three-dimensional (3D) printing is an advanced technology that used for obtaining as a matter the output of a three-dimensional model (Liaw & Guvendiren, 2017; Ngo, Kashani, Imbalzano, Nguyen, & Hui, 2018). This technology allows the manufacturing of customizable, biocompatible, patient-specific, quite comprehensive, mechanically stable and rapidly fabricated products in medical fields (Kogelenberg, Yue, Dinoro, Baker, & Wallace, 2018; Liaw & Guvendiren, 2017). Notably, 3D printed tissue scaffolds are popular in regenerative medicine and tissue engineering applications (Serra, Mateos-Timoneda, Planell, & Navarro, 2013). There are many studies related to 3D printed tissue scaffolds that are based on synthetic and natural polymers in the literature (Jayatissa, Unagolla, & Bhaduri, 2018; Kogelenberg et al., 2018; Konta, García-Piña, & Serrano, 2017; Serra et al., 2013). However, SA-based scaffolds are properly popular in tissue applications.

SA is the most preferred natural anionic polymer that is used for biomedical applications due to its biocompatibility, low toxicity and low cost (Lee & Mooney, 2012). The application of SA as scaffolds could become in the form of hydrogels, films/membranes, and nanofibers (Aderibigbe & Buyana, 2018). For instance, Straccia et al. prepared alginate hydrogels coated with chitosan to delay the releasing of hydrophilic molecules from the alginate matrix (Straccia, d'Ayala, Romano, Oliva, & Laurienzo, 2015). Kamoun et al. displayed that the poly(vinyl alcohol) – alginate hydrogels loaded sodium ampicillin as topical antibiotic could be excellent membrane for wound care (Kamoun, Kenawy, Tamer, El-Meligy, & Eldin, 2015). Also, alginate can be printed three-dimensionally to manufacture scaffolds. Luo et al. prepared 3D printed bone formation peptide-1 (BFP-1) loaded alginate scaffolds for enhanced bone regeneration (Luo, Luo, Gelinsky,

Huang, & Ruan, 2017). Liakos et al. studied the anti-microbial and anti-fungal essential oils (EOs) dispersed SA films to change the antimicrobial activity of alginate polymer. In scaffolds, protection of wounds against unwanted bacteria is a vital situation. Therefore effective substance addition could be an excellent option to prevent the colonization of the wound by bacteria (Liakos et al., 2014).

Propolis (Ps) or bee glue is a resinous substance collected by honey bees from leaf, exudates, bud, etc. of different plants to build, isolate and protect beehives (Keskin, Keskin, & Kolayli, 2019). Generally, it is collected from pine, willow, oak, elm, nectar and pollen materials (Oryan, Alemzadeh, & Moshiri, 2018). The Ps sources, season, collecting time, the difference of locations (geographical differences), illumination, altitude and producing methods can play an important role in changing the physical and chemical properties of Ps (Sharaf & El-Naggar, 2019). There are more than 300 compounds in the Ps, according to the literature (Oliveira et al., 2015). Antimicrobial and antioxidant effect of Ps comes from phenolic compounds. Especially antimicrobial activity of Ps has been widely investigated (ALBAYRAK & ALBAYRAK). The Ps has antibacterial (Bueno-Silva, Marsola, Ikegaki, Alencar, & Rosalen, 2017; Nina et al., 2016; A. V. Oliveira et al., 2017), antiviral (Yildirim et al., 2016), antifungal (Kujumgiev et al., 1999), antioxidant (Mouhoubi-Tafnine, Ouchemoukh, & Tamendjari, 2016), anti-inflammatory (Valenzuela-Barra et al., 2015), antitumor (da Silva Frozza et al., 2017), anaesthetic (ALBAYRAK & ALBAYRAK) and analgesic properties, therefore, it is a good candidate for using as a therapeutic substance in the biomedical field and wound treatment (Martinotti & Ranzato, 2015). The wound healing process is composed of 4 stages; hemostasis, inflammation, proliferation (granulation-contraction), and remodelling steps. Ps plays a role in the initial phase of the wound repair such as hemostasis and inflammation. It is responsible for stimulating the expression of transforming growth factor- β (TGF- β) that regulates nearly all of the cellular events (Moura et al., 2011).

In the literature, there are a few studies related to Ps and SA. Keskin et al. produced alcohol-free Ps-SA microcapsules by the encapsulation method (Keskin et al., 2019). They displayed that the controlled release of Ps active components. In another study, Candido et al. obtained neomycin- an antibiotic that is very popular in diabetic ulcers - and Ps incorporated SA hydrogel as diabetic ulcers' treatment dressing (Juliano, Pala, & Cossu, 2007). They tried both of the hydrogel and the microparticle form of the SA. The microparticles were produced by using the dripping extrusion method, and the hydrogels were prepared by the help of the casting method. In both alginate-based wound dressing forms, Ps and neomycin were used. The researchers showed that all samples are good candidates to use as an absorbent in wound treatments. Furthermore, Juliano et al. studied polymeric films containing Ps (Yang, Zhang, Bhandari, & Liu, 2018). They prepared the Ps added agar, Alginate, Alginate-chitosan based films. Also, they performed antimicrobial tests against *Escherichia coli*, *Staphylococcus aureus*, and *Candida albicans* strains. They suggested that the alginate and alginate-chitosan films were proposed as a vehicle for the buccal delivery of Ps extracts at the end of the study. As clearly seen in the literature, 3D printing technique, SA and Ps are well-known due to their several benefits. The 3D printing method is employed to develop Ps based SA structures for wound dressing applications.

This study aims to construct biocompatible, 3D printed SA scaffolds by adding Ps extract to improve biological and wound healing properties. The optimized Ps incorporated SA solutions were tried to print with different combinations and parameters. The rheological properties of the obtained printing inks such as viscosity, density, and surface tension were investigated. Besides, the mechanical and the morphological features of the 3D printed scaffolds also were characterized. The antibacterial assay of 3D printed, biofunctional SA-Ps scaffolds were investigated. The cytocompatibility of produced SA scaffolds with different amounts of Ps was studied using the MTT test. As mentioned, there is a limited study related to SA-Ps for wound treatment.

2. MATERIALS AND METHODS

2.1 Chemicals

Sodium alginate (SA) with an average molecular weight of 216.121 g/mol was purchased from Sigma-Aldrich (Istanbul, Turkey). Calcium chloride dihydrate ($\text{CaCl}_2 \cdot 2\text{H}_2\text{O}$) was purchased from Merck (Darmstadt, Ger-

many) for using as a crosslinker. The Ps extract was kindly provided from SBS (Scientific Bio Solutions) Incorporated Company, Istanbul, Turkey). PBS (phosphate-buffered saline) pH 7.4 and pH 2.0 solutions were bought from ChemBio Laboratory Research (Istanbul, Turkey).

Mueller Hinton agar (CM0337B, Oxoid, Thermo Fisher, Basingstoke, UK) and Mueller Hinton broth media (CM0405B, Oxoid), 2 μg and 10 μg ampicillin containing disks (CT0002B and CT0003B, Oxoid) were obtained for antibacterial activity assays. *Escherichia coli* ATCC[®] 25922 and *Staphylococcus aureus* ATCC^(x) 29213 standard strains were used for antibacterial testing.

The evaluation of potential cytotoxicity of SA-Ps scaffolds was performed according to the ISO 10993 standard (Biological evaluation of medical devices), part 5 - Tests for in vitro cytotoxicity, using the extract method and the HFFF2 cell line (human dermal fibroblasts). Cells were cultured in DMEM (Dulbecco's Modified Eagle's Medium with 1 g/l glucose, with stable glutamine, with sodium pyruvate, Biowest #L0066) supplemented with penicillin (100 U/ml) and streptomycin (100 $\mu\text{g}/\text{mL}$) (Invitrogen, #15140122), 10% FBS (Fetal Bovine Serum, S. America origin, Biowest, #S1810). Cells were seeded on a 96 well plate at a density of 20k cells/ cm^2 the day before placing the extracts in contact with cells and incubated at 37 °C in a 5% CO_2 humidified atmosphere incubator (Sanyo MCO-19AIC (UV)).

2.2 Preparation of solutions

The SA and SA-Ps solutions in different concentrations were prepared. Firstly, the SA solution polymer was dissolved in distilled water, and 20 ml of 4.5% (w/v) SA solution was prepared at the room temperature. The SA solution was stirred at 1000 rpm nearly 4 hours up to obtain clear appearance. Secondly, different concentrations of SA-Ps solution were prepared. The different amounts were taken from the prepared 4.5% (w/v) SA solution and liquid Ps extract in various amounts were added dropwise to SA solution. The SA-Ps solutions were prepared as 10%, 20% and 40% (v/v) concentrations of Ps. They were named as Sample 1 that is pure SA, Sample 2 (10% v/v Ps content), Sample 3 (20% v/v Ps content) and Sample 4 (40% v/v Ps content) respectively. The SA concentration was stayed constant as 4.5% (w/v). All solutions' total volume was 5 ml. This new combination of SA and Ps incorporated solutions were mixed in stirrer for 30 minutes. 1% (w/v) of $\text{CaCl}_2 \cdot 2\text{H}_2\text{O}$ is used as crosslinker.

2.3 Design and 3D printing of scaffolds

A schematic drawing of the 3D printing process is revealed in **Figure 1**. The scaffolds were designed as square 20 x 20 x 1 mm^3 dimensions using SolidWorks[®]. The roughly drawn scaffold structure is converted into an STL (stereolithography) file that is required file format for 3D printing and transferred to Simplify3D[®] software. The designed scaffolds were printed by using a modified extrusion 3D printer (Ultimaker²⁺, Netherlands) which manipulated from the computer-aided pump part. The digital syringe pump was used to feed the solutions. The nozzle diameter was 0.35 mm. The printing speed was 650 mm/min for control SA scaffolds however 550 mm/min speed was chosen for Ps added SA scaffolds. The scaffolds' infilling percentage was 70%, and the layer was 20 for all scaffolds. The infill pattern was rectilinear with 45-degree angles. These parameters were determined as a result of optimization studies.

The prepared Ps based SA solution was taken to 10 mL syringe for 3D printing. Firstly, the coordinates of the syringe were adjusted and secondly, the glass slide was placed on the table of the 3D printer. After giving the necessary parameters to the program and centring the 3-axis of the printer, SA based scaffolds were printed. The CaCl_2 crosslinker solution was used to printed scaffold for crosslinking and easily removing. The scaffolds were exposed to the CaCl_2 for 15 minutes. After completely drying, the printed material was removed from the glass slide carefully by the help of a lancet blade. During the experiment, the temperatures were set at the room temperature but a fan was used to accelerate for proper drying.

2.4 Characterizations

2.4.1 Physical properties characterization

The density, viscosity, and surface tension of the solutions were determined. The density of control SA and

Ps incorporated SA solutions were determined by using a 10 mL standard pycnometer. The surface tension of the solutions was measured with a force tensiometer (Sigma 703D, Attension, Germany). The viscosity of solutions was founded by a digital viscometer (DV-E, Brookfield, USA). Each equipment was calibrated before the tests, and all samples were tested three times.

2.4.2 Fourier transform-infrared spectroscopy (FT-IR)

Chemical characterization of scaffolds was performed by Fourier Transform Infrared (FT-IR) Spectrometer (Jasco, FT-IR 4700). The FT-IR spectra of samples were founded at the scanning range of 400 and 4000 cm^{-1} and a resolution of 4 cm^{-1} .

2.4.3 Scanning electron microscopy (SEM)

The morphological characterization of scaffolds was also performed with scanning electron microscopy (SEM, EVA MA 10, ZEISS, USA). The samples' surfaces were coated with gold before imaging to obtain a conductive surface. The average pore size and distribution of the pores for each sample were determined by the help of image software (Olympus AnalySIS, USA).

2.4.4 Mechanical properties of the scaffolds

The tensile test of the scaffolds was carried out by a tensile test machine (SHIMADZU, EZ-LX, CHINA). The thickness and length of the scaffolds were measured by a digital micrometer (Mitutoyo). The three samples from SA and SA-Ps scaffolds were measured. All samples were placed uniaxial to the appropriate section of the device from their upper and lower positions.

2.4.5 *In-vitro* release profile of Ps

A standard calibration curve is a necessary graph for determining the unknown concentrations. Therefore, this curve was prepared before starting the release test. The solutions containing different Ps ratios were prepared and measured spectrophotometrically by UV-1280 at 200-400 nm. The highest absorbance values and wavelength of Ps were determined to draw a standard calibration curve. The solutions' absorbance graph was founded in **Figure 4(a)**. The standard calibration curve was also drawn, as shown in **Figure 4(b)**.

The release profile of Ps from 3D printed scaffold was determined in PBS (pH 2.0 and pH 7.4) buffer solutions. The sliced scaffolds (9 mm x 9 mm) were placed into 2 ml PBS buffer solutions medium. Samples were incubated at 37 degC in a thermal shaker (BIOSAN TS-100) at 250 rpm. The release profile of Ps was performed in the time intervals of 5 minutes until the first 30 minutes and then up to 240 minutes at half an hour intervals. The 1 ml of solutions were taken from PBS solutions and replaced with 1 ml of fresh PBS solutions. The taken solutions were measured spectrophotometrically by UV-1280 (SHIMADZU, 200-400 nm). The cumulative releasing percentage was calculated by the help of the standard calibration curve of Ps, as shown in **Figure 4(c)**.

2.4.6 Ps release kinetics

In order to investigate the Ps release mechanism from 3D printed scaffolds, Ps release profiles were fitted two popular kinetic models as Higuchi and Peppas Korsmeyer (Power Law) equations. (Eq 1-2)

Higuchi equation defines a linear dependence of the active fraction released per unit of the square of time.

$$\underline{Q = K_h t} \quad (1)$$

where Q is the fractional amount of Ps released at time t and K_h is release rate constant.

The equation of Korsmeyer–Peppas is

$$\underline{Q = K t^n} \quad (2)$$

where Q is the fractional amount of Ps release at time t, K is the kinetic constant and n is the diffusion exponent which is indicative of the drug release mechanism.

The interpretation of the release mechanism by the n value depends according to the geometry of the matrix. For a cylindrical system, when n approximates to 0.45 Fickian diffusion is implied and $0.45 < n < 1$ refers to the Non-Fickian diffusion.

2.4.7 Swelling and degradation behaviours of scaffolds

The scaffolds were sliced equally and placed into 2 ml PBS solution (pH=7.4). They were incubated in a thermal shaker at 37°C. The swollen scaffolds' weight was measured after removing excess water by filter paper. The swelling test was measured at half-minute intervals of 300 min. Also, the swelling ratio was calculated by using equation 3 (C. Gao, Liu, Chen, & Zhang, 2009):

$$SR = \frac{W_t - W_0}{W_0} \quad (3)$$

Here, W_t is swollen samples; W_0 is samples' weight before swelling.

The degradation (weight loss) of scaffolds was performed in plastic eppendorf filled with 2 ml PBS solution (pH=7.4). The degradation tests were also conducted in a thermal shaker at 37°C. The swollen scaffolds were removed from PBS medium, washed with distilled water and dried at room temperature for 2.5 hours at predetermined time intervals. The degradation was determined by measuring weight loss (%) by using equation 4:

$$\text{Weight loss (\%)} = \frac{W_1 - W_2}{W_1} \times 100 \quad (4)$$

Here, W_1 and W_2 are the weights of the scaffolds before and after degradation, respectively.

2.4.8 Antibacterial assay

Overnight cultures of *E. coli* ATCC® 25922, and *S. aureus* ATCC(r) 29213 in Mueller-Hinton broth were used to prepare bacterial suspensions within the same broth and adjusted to 0.5 McFarland turbidity standard ($1-2 \times 10^8$ CFU/mL). Resulting bacterial suspensions were inoculated on Mueller-Hinton agar plates by using an automated plate inoculator. Disks (5 mm in diameter) were cut from Ps containing scaffolds and hold for 1 hour under UV light (254 nm) for sterilization. Sterilized disks were placed on the surface of bacteria inoculated Mueller-Hinton agar plates with a sterile forceps. Ampicillin containing disks (2 and 10 µg) was used as a positive control for *S. aureus* ATCC® 29213 and *E. coli* ATCC(r) 25922, respectively. Plates were incubated at 37degC for 18 h, and growth inhibition zones around disks were measured and evaluated.

2.4.9 Cell cytotoxicity

The extracts were prepared using a mass of material to the volume of the culture medium of 20 mg/ml for the SA scaffolds and 5 mg/ml for the SA with Ps scaffolds. The latter scaffolds have a mass ratio of Ps to SA of 0.3:1.0. Scaffolds were sterilized by exposure to UV radiation from the UV lamp of a biological safety cabinet (ESCO Labculture II) for 30 min each side. The extraction conditions were: 48 h at 37 degC. Then, the cell culture medium was aspirated and the extracts placed in contact with cells. Extracts were serially diluted by factor of two in order to prepare equivalent concentrations of 10, 5 and 2.5 mg/ml for the SA scaffold's extract and 2.5, 1.25, 0.63, 0.31, 0.16, 0.08 and 0.04 mg/ml. For each concentration, 4 replicates were prepared. Negative (viable cells) and positive (cells in a cytotoxic environment) controls were established by culturing cells with normal medium and medium supplemented with 10% Dimethyl sulfoxide (DMSO), respectively. The extracts remained in contact with cells for 48h. Finally, the cell population was evaluated using the resazurin assay (Vieira, Silva, do Rego, Borges, & Henriques, 2019). All media were replaced by a 1:1 mixture of culture medium and a resazurin solution (0.04 mg/mL in PBS). After 2 h of incubation in the CO₂ incubator, medium absorbance was measured at 570 nm and at 600 nm with a microplate reader (Biotex ELX 800UV).

2.4.10 Statistical analysis

All data were presented as mean \pm standard deviation (SD). The statistical analysis was performed using SPSS software with p -value ≤ 0.05 considered statistically significant. All measurements were performed in duplicates and their mean values were taken as the final result.

3. RESULTS AND DISCUSSION

3.1 Optimization and characterization of solution

The optimum parameters of the solution for the producing 3D structure were investigated, and the optimized solution was chosen according to their density, viscosity, and surface tension properties. Especially, the viscosity of the solution is the most important parameter for the 3D printing process. The solution with high viscosity would possibly clog the needle tip and causes the preventing of next layer printing. In contrast to high viscosity, if the solution viscosity is too low, the printed strands tend to spread. Thus the two adjacent layers would join together, and the next layers collapse due to merge. Therefore, the viscosity of the solutions must be properly adjusted and selected for 3D printing (You, Wu, & Chen, 2017). In addition to viscosity, surface tension is also an important parameter. There is a relation between surface tension and droplet. If the surface tension of the resin or solution is too high, the solution will not be jetted through the nozzle. In contrast to this, if the surface tension is too low, the droplet shape would be changed and the non-uniform droplets will exist instead of cohesive droplets (Chua, Wong, & Yeong, 2017).

The prepared SA and Ps incorporated SA solutions' viscosity, surface tension and density were measured. The effect of viscosity, density and surface tension on the scaffolds is demonstrated in **Table 1**. The all 3D printed scaffold images were in the same magnification. Sample 3 has the highest viscosity and surface tension than other solutions according to results. When the Ps content increases, the viscosity and surface tension increases simultaneously, as shown in **Table 1**. As above stated, a certain level of increment in viscosity provides a positive effect on printability (Ergul et al., 2019). Also, the Ps is a resinous substance; therefore the more amount of the Ps would increase the viscosity and surface tension of the solutions due to stickiness. Sample 4 was not appropriately produced due to the high viscosity of the solution. The high viscosity solution would cause the printability problems (Ouyang, Yao, Zhao, & Sun, 2016). For instance, the solution infrequently comes that causes to destroyed pore shapes. Also, filaments would be thicker and close the pores due to the viscosity. The desired scaffold shape will not be obtained, as shown in **Table 1**. In addition to surface tension and viscosity parameters, there was no significant difference between each sample for density. The viscosity and surface tension of optimized solution was chosen as Sample 3 (4.5% w/v SA-20% v/v Ps solution) for 3D printing of scaffolds. The production and experiments were carried out with optimized solutions.

3.2 Fourier transform infrared spectroscopy (FT-IR)

FT-IR is a chemical analysis that is used to determine polymer (SA) and effective substance (Ps) interaction. Both FT-IR spectra of SA and SA-Ps scaffolds were shown in **Fig.2**. For pure SA, absorption bands are related to some functional groups such as hydroxyl, ether and carboxylic functional groups (Daemi & Barikani, 2012). SA shows characteristic stretching vibrations of O-H peak at 3334 cm^{-1} also literature proves that this characteristic band is found in the range of $3000\text{-}3600\text{ cm}^{-1}$ (Daemi & Barikani, 2012; Pereira, Tojeira, Vaz, Mendes, & Bartolo, 2011). Asymmetric stretching vibration of $-\text{COO}-$ groups peak at 1593 cm^{-1} also symmetric stretching vibration of $-\text{COO}-$ groups peak at 1419 cm^{-1} and $-\text{C-O-C}-$ stretching vibration peak at 1078 cm^{-1} are obtained (Cesur et al., 2019; Mimmo, Marzadori, Montecchio, & Gessa, 2005; Zheng et al., 2016).

The FT-IR spectrum of Ps was shown in **Figure 2(b)**. It is nearly similar to pure SA. For instance, Ps showed O-H stretching vibration peak at 3344 cm^{-1} due to ethanol. C-H stretching vibration peak at 2974 and 2927 cm^{-1} due to CH_2 and CH_3 bands, C=C stretching vibration peak found at 1637 cm^{-1} due to aromatic ring deformations also it is a typical peak of resins. However, according to literature, this peak would be probably related to stretching vibration of C=C and C=O groups where the flavonoids and amino acids. The $-\text{C-H}-$ bending vibration and aromatic stretching vibration peaks were observed at 1450 cm^{-1} . The $-\text{C-H}-$ bending peak in CH_3 also was seen at 1377 cm^{-1} , but sometimes this peak was non-identified according

to some studies (Renata Nunes Oliveira et al., 2016). The band at 1271 cm^{-1} would be probably associated with C-O group of polyols and also related to C-H bending. This peak is typical for resins. The C-O-C stretching and C-F stretching vibration peaks were obtained at 1146 cm^{-1} . The C-O stretching peak from esters and C-O-C stretching vibration peak were found at 1086 cm^{-1} . The peak at 1086 cm^{-1} can be related to secondary alcohol while the peak at 1043 cm^{-1} would be related with both primary and secondary alcohol. Finally, the peak at 878 cm^{-1} was normally non-identified, but probably there is a relation between C-C stretching vibration (Hussein et al., 2017; Martin-Ramos et al., 2018; Renata Nunes Oliveira et al., 2016).

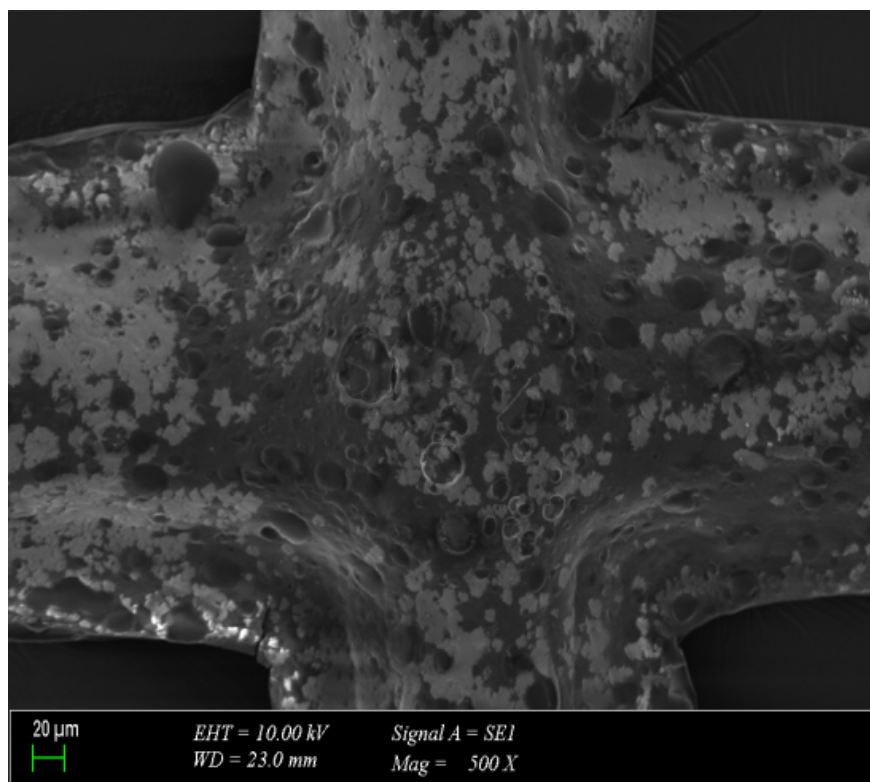
As shown in **Figure 2**, SA and Ps characteristic peaks were displayed for 3D printed scaffolds. The integration of Ps and SA was successfully achieved according to these peak results.

3.3 SEM results

The size and structure of pores are important factors for tissue scaffold applications. The three-dimensional porous scaffold provides cell adhesion and proliferation. Cells move easily to repair zone during the wound healing process thanks to these pores. Open and interconnected pores are necessary for mechanical support, cell nutrition, the permeability of gases and removal of toxic substances (by-products) from tissues (Lu, Oh, Kawazoe, Yamagishi, & Chen, 2012). If the porosity is high, it would provide more nutrients' transport to tissues but results with lower structural density due to reduced mechanical stability (Egan, 2019). Normally, it is very difficult to say that optimal pore size values in tissue scaffolds due to different types of tissues and cell diversity. However, some optimum pore size ranges proposed for different kinds of cells and tissues (Oh, Park, Kim, & Lee, 2007). For instance, Yannas et al. displayed that 20-125 μm pore size is optimal for skin regeneration (Yannas, Lee, Orgill, Skrabut, & Murphy, 1989). The pore size of 100-400 μm is acceptable for bone tissues (Boby, Stackpool, Hacking, Tanzer, & Krygier, 1999; Zardiackas et al., 2001). Salem et al. explained that a 40-150 μm pore size range is better for fibroblast binding (Salem et al., 2002). Also, porosity depends on used material; therefore the certain pore size range is really difficult.

The scaffolds' SEM images, pore size histograms and pore size distribution according to propolis content were shown in **Figure 3 (a,b,c,d,e)**. Results demonstrated that average pore size distributions of Sample 1 was in 208 μm and the surface was smooth **Figure 3(a)**. The average pore sizes for Sample 2 and Sample 3 were in 202 μm and 172 μm respectively and surfaces were rough due to some agglomerated Ps powders as shown in **Figure e**. The roughness is beneficial for cell attachment and proliferation (Naseri et al., 2016; Sultan & Mathew, 2018). When the Ps content was increased, the pore sizes were decreased. The decreasing in average pore sizes can be explained due to filling the pores with Ps (Oliveira, McGuinness, Ramos, Kajiyama, & Thiré, 2016). The Ps diffuses to the pore walls and increases the wall thickness of the scaffolds. The adjacent filaments will be closer to each other. Therefore the pores were smaller than Sample 1 (pure SA). Sutjarittangtham et al. showed that fiber diameters were decreased by the addition of different concentrated Ps. The fiber diameters were decreased from 140-190 nm to 60-70 nm due to high Ps content (Sutjarittangtham et al., 2012).

Normally, the scaffolds were designed as $20 \times 20 \times 1\text{ mm}^3$ (X, Y, Z dimensions). However, the dimensions were measured as $18 \times 18 \times 0.08\text{ mm}^3$. The difference between the designed and produced scaffolds' dimensions may result from the cross-linking process with CaCl_2 . Gao et al. studied that the dual crosslinking effect on alginate hydrogel microfibers (Y. Gao & Jin, 2019). In this experiment, high CaCl_2 concentration means high Ca cations and these ions interchange the alginate fibers in "egg-box" structure due to sodium and calcium ions interaction. The alginate strands formed a cooperative binding structure which ensures the increasement of alginate gels' tightness. Therefore, the crosslinking can be shown as a reason for shrinking of the dimensions by increasing of the structure tightness (Simpson, Stabler, Simpson, Sambanis, & Constantinidis, 2004).



3.4 Tensile properties of 3D printed scaffolds

Structural properties of porous scaffolds, such as pore sizes and porosity, are important for their mechanical properties as well as for nutrient transport and may affect their potential performance after introduction into the defect site (Stangl, Rinne, Kastl, & Hendrich, 2001). A tensile test was performed to analyze the effects of mechanical properties on printed scaffolds. The tensile properties of all scaffolds were examined at room temperature. The tensile strength results distribution for each three sample as follows, respectively were (3.92 ± 1.08 MPa), (2.42 ± 0.62 MPa) , (2.33 ± 1.76 MPa). Strain at break percentages were ($14.74 \pm 1.22\%$) for Sample 1, ($20.57 \pm 1.96\%$) for Sample 2, and ($25.00 \pm 6.68\%$) for Sample 3. These results are crucial in determining the flexibility of the product to achieve successful wound treatment (M. C. Straccia, 2014). The results clearly showed that the tensile strength of Sample 1 has a maximum tensile strength (3.92 ± 1.08 MPa) and minimum tensile values ($14.74 \pm 1.22\%$) compared to the others. With the addition of different proportions of Ps to SA, tensile strength decreased from 3.92 MPa to 2.33MPa. Elongation at break (%) increased from 14.74 to 25. The reason for this situation is that Ps has plasticizing properties (Bodini, Sobral, Fávoro-Trindade, & Carvalho, 2013). When the effect of pore size on mechanical properties was examined, scaffolds having a pore size of 208 μm (Sample1), 202 μm (Sample 2) and 172 μm (Sample 3) caused significant differences in the tensile strength values of the produced scaffolds. As Ps was incorporated into SA, it would normally be expected that the smaller the pore, the tighter structure, the higher tensile strength. This is due to the fact that the bond structure of the pure SA polymer is stronger than the bond structure between SA-Ps (Chang-Bravo, López-Córdoba, & Martino, 2014).

3.5 *In-vitro* releasing of Ps

The release test of Ps was tested in 2 different media, one of them is near the acidic value (pH=2.0) and the other one is near the basic value (pH=7.4) The samples were taken in every five minutes up to first thirty minutes. After that, the sample was taken in every thirty minutes until 240 minutes (4 hours). As shown in **Figure 4** , there is a fast releasing in pH 7.4 medium than pH 2.0 buffer solution. The release at pH 7.4

lasted for about 240 minutes (about 4 hours) while the release at pH 2.0 lasted for 120 minutes (about 2 hours). The Ps was released nearly 96.43% at pH 2.0 within 2 hours. However, the cumulative releasing of Ps reached up to nearly 97.80% at pH 7.4 within 4 hours. It seems that the releasing of Ps at pH 7.4 is a good candidate for controlled drug delivery systems. These results are convenient with literature. Zhang et al. showed that 90% of Ps was quickly diffused into the simulated gastric fluid (its pH is close to 2.0) within 1 hour and the rest of Ps was diffused into the simulated intestinal fluid (its pH is close to nearly 7.0) due to hydrophilic phenolic compounds (Hao Zhang et al., 2018). Juliano et al. obtained that polyphenols slowly release and reach 96.3% value for maximum releasing after 2 hours from SA capsules at pH 7.0 (Juliano et al., 2007). In another study, the fast release profile of Ps was observed at the beginning of the experiment. However, the *in-vitro* release still was controlled despite Ps concentration increased (Sharaf & El-Naggar, 2019). In our results, also rapid and controlled release was observed.

The wound healing is a complex process. There is a relation between the pH and wound-milieu. All biochemical processes are affected by the pH of the media. The studies showed that there is a shift toward an acidic pH, forming during wound healing stages (Uzun, Anand, & Shah, 2012). The continued release of drugs or effective substance during this pH changing is a considerable state. Therefore, 3D printed, SA-Ps tissue scaffolds show a rapid release profile even in acidic environments, which once again shows their suitability for using as a wound dressing in wound treatments.

3.6 Ps release kinetics results

In vitro Ps release from 3D scaffolds has been investigated in two different pH values and the release data were fitted to two different models for the purpose of determining Ps release mechanism. The correlation coefficients R^2 obtained for each model is shown in **Table 2**. Highest R^2 values (0.9822 and 0.9515) were obtained from Higuchi kinetics, which means that the release of Ps is controlled by diffusion through the polymeric scaffolds, obeying Fick's laws (1st and 2nd). When Ps release was fitting to Korsmeyer-Peppas equation, R^2 values were 0.9715 and 0.8633 in neutral and acidic medium, respectively. It can be seen that the release mechanism of Ps follows Fickian diffusion by $n \sim 0.45$ only in neutral medium. The Korsmeyer-Peppas kinetic is not suitable to use for the acidic medium because of the low R^2 . This may be due to the faster release of Ps from the SA matrix. The similar results were obtained in the previous studies (Jaya, Durance, & Wang, 2009; Torre et al., 1998)

3.7 Swelling and degradation tests of scaffolds

The water absorption or swelling ability of tissue scaffolds is an important parameter that allows body fluids, wound exudates absorption and transfer of cell nutrients inside the scaffold. The swelling under physiological conditions should be controlled to prevent rapid degradation and mechanical weakening of tissue scaffolds (Maji, Dasgupta, Pramanik, & Bissoyi, 2016). As shown in **Figure 5(a)**, there is a high swelling ratio in the first phases of both samples (Sample 1 and Sample 3). This swelling is probably caused by the entrance of PBS to the scaffold fibers (Renata N Oliveira et al., 2016). The swelling ratio of Sample 1 is bigger than Sample 3 scaffold. Normally, it is known that alginate dressings have a high water uptake capacity (Boateng, Matthews, Stevens, & Eccleston, 2008; B. Gupta, Agarwal, & Alam, 2010). However, there is a decreasing swelling by the addition of Ps into the SA scaffolds in this study. Oliveira et al observed that Ps causes less space for water uptake by filling the pores, thereby reducing the stretching in the fibers with less water (Renata N Oliveira et al., 2016). Candido et al. also showed that the addition of Ps and the interaction of SA chains with Ps result in low water absorption (Candido et al., 2019). Not only the addition of Ps but also the pore structure is one of the most important parameters affecting water uptake. High porosity structure provides high water uptake (N. V. Gupta & Shivakumar, 2012; R. N. Oliveira et al., 2017). The high swelling ratio in Sample 1 could be explained by the fact that the pores in Sample 1 (208 μm) are bigger than the pores in Sample 3 (172.81 μm). Therefore, the swelling ratio in Sample 3 is lower than the swelling ratio in Sample 1 due to the addition of Ps and the reduced porosity.

The degradation of tissue scaffolds is a critical parameter during the tissue regeneration process (Hongbo Zhang, Zhou, & Zhang, 2014). The scaffolds should be able to have an appropriate degradation rate up to

the new extracellular matrix (ECM) is steady (Kamoun et al., 2015). Sample 1' and Sample 3's degradation tests were performed in PBS (pH 7.4) at 37°C by measuring the weight loss percentage. As shown in **Figure 5(b)**, the degradation lasted 7 days (168 hours). The weight loss in Sample 1 approaches to 60% percent and the weight loss in Sample 3 reaches nearly 50% percent at the end of 7 days. As in swelling, the highest weight loss percentage was observed in Sample 1. The first reason can be explained by the swelling capacity for this situation. Sample 1 had the highest swelling capacity than Sample 3. The samples' swelling ability causes to more freedom of amorphous chains to move easily. If there is no cross-linking, the fibers could be ruptured from the structure by the help of media and accelerate the weight loss (Kamoun et al., 2015; Renata N Oliveira et al., 2016). Therefore, Sample 1's chains tend to easily break down during degradation tests due to high swelling capacity even if it was cross-linked. Secondly, the pore structure affects degradation and weight loss rate. There is a direct relationship between the pore size and swelling capacity. Therefore, degradation is observed more rapidly and highly due to the high water absorption ability of scaffolds and weakening of mechanical properties in highly porous structures. Also, Odelius et al. displayed that the degradation rate of porous structures decreased with decreasing pore size (Odelius et al., 2011). Thirdly, the weight loss in Sample 3 resulted from the Ps releasing because hydrolytic degradation accelerates the Ps releasing with weight loss (Candido et al., 2019). Still, this weight loss percent was not more significant than Sample 1's weight loss percent due to highly absorbent property of SA polymers.

3.8 Antibacterial assay results

Antibacterial activity of SA-Ps scaffolds was determined by disk diffusion assay, and the results are shown in **Figure 6** and **Table 3**. None of the Ps incorporated samples could exhibit a zone of inhibition for *E. coli* ATCC® 25922 strain. Also, SA disks without Ps did not show any antibacterial effect against *E. coli* ATCC(r) 25922, and *S. aureus* ATCC(r) 29213. Zones measured around ampicillin disks (2 µg and 10 µg) for both bacterial strains were in the expected range according to EUCAST criteria ("Breakpoint tables for interpretation of MICs and zone diameters. Version 9.0," 2019). Moreover, disks containing different concentrations of Ps exhibited significant antibacterial activity against *S. aureus* ATCC® 29213, which was comparable with ampicillin (Figure 8).

The *S.aureus* and *E.coli* bacteria are the most popular bacteria types among hospital bacterias. Therefore, nearly all materials' antibacterial tests were performed with these two types of bacterias. However, not only these two types of bacteria but also *Salmonella spp.* and *P.aeruginosa* are other types of bacteria used for determining of Ps antibacterial activity. The antibacterial activity of Ps against *S.aureus* was proved with some studies. Arikan et al. studied Ps added electrospun fabrics' antibacterial activity against both Gram-positive (*S.aureus*) and Gram-negative bacteria (*A. Baumannii* and *P.aeruginosa*)(Arikan & Solak, 2017). The fabrics displayed antibacterial activity against *S.aureus*, but it was not provided antibacterial activity against Gram-negative bacterias. In another study, Silici et al. showed that ethanolic extract of different Ps samples displayed high antibacterial activity against Gram-positive cocci (*S.aureus*) however had a weak antibacterial activity against Gram-negative bacteria (*E.coli* and *P. Aeruginosa*)(Silici & Kutluca, 2005). Also, Akca et al. showed that Ps was more effective inhibiting of Gram-positive bacteria than Gram-negative bacteria in their biofilm state (Akca et al., 2016). The antibacterial activity of Ps could be considered in two stages (Przybyłek & Karpiński, 2019). Firstly, it shows directly effect on microorganisms and secondly, Ps stimulates immune system resulted in activation of natural defences of microorganisms (Bankova, Christov, & Tejera, 1998). Ps affects cellular membrane permeability of microorganisms and disrupts membrane potential. It results in reduced adenosine triphosphate (ATP) production and decreasing bacterial mobility. However, the species-specific outer membrane structure of the microorganisms is also another important criteria for presenting the antibacterial activity of Ps. For instance, The Gram-negative bacteria have some hydrolytic enzymes that degrade active components of Ps. Therefore, the antibacterial activity of Ps is lower in Gram-negative bacteria than Gram-positive bacteria (Kedzia & Holderna-Kedzia, 2013; Sforcin, 2016). In this study, also the antibacterial activity of Ps was observed in *S.aureus* strains due to different outer membrane structure of microorganisms. The results were aligned with literature and therefore Ps is a good candidate and alternative instead of drugs as an antibacterial preservative for wound healing processes.

3.9. Cell cytotoxicity evaluation

Figure 7 shows the relative cell population for the different extracts and concentrations and for the negative and positive cell controls. When relative populations are above 90%, the extracts are considered non-cytotoxic. This happens for all extracts obtained with SA scaffolds, which means that these extracts are non-cytotoxic up to at least a concentration of 20 mg/ml. For the extracts obtained with the Ps-containing scaffolds, the highest non-cytotoxic concentration is 0.08 mg/ml. Given the Ps to SA mass ratio, this concentration corresponds to Ps concentration of 18.5 $\mu\text{g/ml}$ in the extracts, provided Ps contained in the scaffolds are totally released to the culture medium. At 0.16 mg/ml the extract is slightly cytotoxic and at 0.31 and 0.62 mg/ml the extracts are moderately cytotoxic. At 1.25 mg/ml (which corresponds to a maximum Ps concentration of 288 $\mu\text{g/ml}$) and above the extracts are severely cytotoxic. These results are aligned with other results already reported in the literature. Frozza et al. (da Silva Frozza et al., 2013) and Silva et al. (Silva et al., 2017) investigated the *in vitro* cytotoxic activity of red Ps from Sergipe, Brazil. Frozza et al. found that short term (1h and 24h) exposure to hydroalcoholic extracts had inhibitory effects on tumor cells (human laryngeal epidermoid carcinoma, Hep-2) corresponding to IC_{50} values of $128 \pm 5 \mu\text{g/ml}$ and $63.5 \pm 3.3 \mu\text{g/ml}$, respectively, while for normal cells (human embryonic kidney, Hek-293) the IC_{50} was in excess of 150 $\mu\text{g/ml}$ for both exposure periods (da Silva Frozza et al., 2013). Silva et al. observed that cell exposure to ethanolic extracts during 72h resulted in IC_{50} values for the glioblastoma (SF-295) tumor cell line of $13.7 \pm 2.5 \mu\text{g/ml}$ and $18.5 \pm 3.4 \mu\text{g/ml}$ for two different Ps lots whereas the colon tumor cells (HCT-116) were less sensitive to Ps extracts, with IC_{50} values ranging from 14.4 to 41.6 $\mu\text{g/ml}$ (Silva et al., 2017). Calhelha et al. (Calhelha, Falcão, Queiroz, Vilas-Boas, & Ferreira, 2014) evaluated the cytotoxicity of phenolic extracts from Portuguese Ps of different origins using human tumor cell lines and porcine liver non-tumor primary cells. Growth inhibition was evaluated after exposing cells to Ps extracts for 48 h. Cytotoxic doses for tumor and normal cells were in close proximity and typically in the interval, 30 to 50 $\mu\text{g/ml}$ with the exception of the HCT15 (colon carcinoma) cells for whom GI_{50} values as low as 10 $\mu\text{g/ml}$ were obtained for some of the Ps extracts studied.

Although the Ps concentrations used in the production of scaffolds in this work may lead to the presence of Ps in the wound fluid at concentrations above the inhibitory concentrations reported in the literature and the cytotoxicity threshold determined in this work, it is important to note that the anti-microbial effect is most important and necessary upon dressing application to a wound and as time passes the wound exudates will wash the excess Ps away from the wound and conduce to an environment where cells can proliferate and proceed into the tissue formation and remodelling phases of wound healing.

4. CONCLUSIONS

In this study, Ps added SA scaffolds were successfully developed and produced by a modified extrusion 3D printer. Sodium alginate was chosen as a polymer due to its important parameters for tissue engineering applications. Also, propolis was used as an active biological substance that has a high potential for wound healing application because of its antimicrobial effect. Different concentrations of SA and Ps were mixed and the optimum concentrations were determined according to physicochemical parameters for the 3D printing process. The optimized scaffold was determined as Sample 3 (4.5 % wt and 20% v/v) and the deep experiments were carried out on this combination. The highest mechanical properties were observed in Sample 3. The desired morphological and biological properties were also obtained by Sample 3. The scaffold pore size of Sample 3 was found to be 172 μm that means it is too close to 150 μm , which is required pore size of fibroblast cells binding for wound healing. The antimicrobial results were properly close to well-established ampicillin antibiotics as a control substance. Moreover, cell cytotoxicity analyses were studied. The results showed that the Ps added scaffolds were non-toxic at low concentrations. Considering the results produced in this study, the 3D printed Ps reinforced SA scaffolds have promising properties, and it can be employed as biomaterials for further tissue engineering applications.

ACKNOWLEDGEMENTS

This study was supported by Marmara University FEN-C-YLP-130319-0065 BAPKO Project.

CONFLICT OF INTEREST

The authors have declared no conflict of interest.

ORCID

Muhammet Uzun **ORCID iD** <https://orcid.org/0000-0001-8669-7686>

REFERENCES

- Aderibigbe, B. A., & Buyana, B. (2018). Alginate in wound dressings. *Pharmaceutics*, 10 (2), 42.
- Akca, A. E., Akca, G., Topçu, F. T., Macit, E., Pıkdöken, L., & Özgen, I. Ş. (2016). The comparative evaluation of the antimicrobial effect of propolis with chlorhexidine against oral pathogens: An in vitro study. *BioMed research international*, 2016 .
- ALBAYRAK, S., & ALBAYRAK, S. PROPOLIS: NATURAL ANTIMICROBIAL MATTER. *Ankara Üniversitesi Eczacılık Fakültesi Dergisi*, 37 (3), 201-215.
- Arkan, H. K., & Solak, H. H. (2017). Propolis Extract-PVA Nanocomposites of Textile Design: Antimicrobial Effect on Gram Positive and Negative Bacterias. *International Journal of Secondary Metabolite*, 4 (3, Special Issue 1), 218-224.
- Bankova, V. S., Christov, R., & Tejera, A. D. (1998). Lignans and other constituents of propolis from the Canary Islands. *Phytochemistry*, 49 (5), 1411-1415.
- Boateng, J. S., Matthews, K. H., Stevens, H. N., & Eccleston, G. M. (2008). Wound healing dressings and drug delivery systems: a review. *Journal of pharmaceutical sciences*, 97 (8), 2892-2923.
- Bobyn, J., Stackpool, G., Hacking, S., Tanzer, M., & Krygier, J. (1999). Characteristics of bone ingrowth and interface mechanics of a new porous tantalum biomaterial. *The Journal of bone and joint surgery. British volume*, 81 (5), 907-914.
- Bodini, R. B., Sobral, P. J. d. A., Fávoro-Trindade, C. S., & Carvalho, R. A. d. (2013). Properties of gelatin-based films with added ethanol-propolis extract. *LWT-Food Science and Technology*, 51 (1), 104-110.
- Breakpoint tables for interpretation of MICs and zone diameters. Version 9.0 (2019).
- Bueno-Silva, B., Marsola, A., Ikegaki, M., Alencar, S. M., & Rosalen, P. L. (2017). The effect of seasons on Brazilian red propolis and its botanical source: chemical composition and antibacterial activity. *Natural product research*, 31 (11), 1318-1324.
- Calhelha, R. C., Falcão, S., Queiroz, M. J. R., Vilas-Boas, M., & Ferreira, I. C. (2014). Cytotoxicity of Portuguese propolis: the proximity of the in vitro doses for tumor and normal cell lines. *BioMed research international*, 2014 .
- Candido, J. D. C., Conceição, N. A., Moreira, A. P. D., Calçada, L. A., Araújo, L. S., dos Santos, R. A., . . . Castro, R. N. (2019). Alginate hydrogels incorporating neomycin or propolis as potential dressings for diabetic ulcers: Structure, swelling, and antimicrobial barrier properties. *Polymers for Advanced Technologies* .
- Cesur, S., Oktar, F. N., Ekren, N., Kilic, O., Alkaya, D. B., Seyhan, S. A., . . . Erdemir, G. (2019). Preparation and characterization of electrospun polylactic acid/sodium alginate/orange oyster shell composite nanofiber for biomedical application. *Journal of the Australian Ceramic Society* , 1-11.
- Chang-Bravo, L., López-Córdoba, A., & Martino, M. (2014). Biopolymeric matrices made of carrageenan and corn starch for the antioxidant extracts delivery of Cuban red propolis and yerba mate. *Reactive and Functional Polymers*, 85 , 11-19.

Chua, C., Wong, C., & Yeong, W. (2017). Chapter Five-Material Characterization for Additive Manufacturing *Standards, Quality Control, and Measurement Sciences in 3D Printing and Additive Manufacturing* (pp. 95-137): Academic Press.

da Silva Frozza, C. O., Garcia, C. S. C., Gambato, G., de Souza, M. D. O., Salvador, M., Moura, S., . . . Borsuk, S. (2013). Chemical characterization, antioxidant and cytotoxic activities of Brazilian red propolis. *Food and chemical toxicology*, *52* , 137-142.

da Silva Frozza, C. O., Santos, D. A., Rufatto, L. C., Minetto, L., Scariot, F. J., Echeverrigaray, S., . . . Borsuk, S. (2017). Antitumor activity of Brazilian red propolis fractions against Hep-2 cancer cell line. *Biomedicine & Pharmacotherapy*, *91* , 951-963.

Daemi, H., & Barikani, M. (2012). Synthesis and characterization of calcium alginate nanoparticles, sodium homopolymannuronate salt and its calcium nanoparticles. *Scientia Iranica*, *19* (6), 2023-2028.

Egan, P. F. (2019). Integrated design approaches for 3D printed tissue scaffolds: Review and outlook. *Materials*, *12* (15), 2355.

Ergul, N. M., Unal, S., Kartal, I., Kalkandelen, C., Ekren, N., Kilic, O., . . . Gunduz, O. (2019). 3D printing of chitosan/poly (vinyl alcohol) hydrogel containing synthesized hydroxyapatite scaffolds for hard-tissue engineering. *Polymer Testing*, *79* , 106006.

Gao, C., Liu, M., Chen, J., & Zhang, X. (2009). Preparation and controlled degradation of oxidized sodium alginate hydrogel. *Polymer degradation and stability*, *94* (9), 1405-1410.

Gao, Y., & Jin, X. (2019). Dual Crosslinked Methacrylated Alginate Hydrogel Micron Fibers and Tissue Constructs for Cell Biology. *Marine drugs*, *17* (10), 557.

Gupta, B., Agarwal, R., & Alam, M. (2010). Textile-based smart wound dressings.

Gupta, N. V., & Shivakumar, H. (2012). Investigation of swelling behavior and mechanical properties of a pH-sensitive superporous hydrogel composite. *Iranian journal of pharmaceutical research: IJPR*, *11* (2), 481.

Hussein, U., Hassan, N., Elhalwagy, M., Zaki, A., Abubakr, H., Nagulapalli Venkata, K., . . . Bishayee, A. (2017). Ginger and propolis exert neuroprotective effects against monosodium glutamate-induced neurotoxicity in rats. *Molecules*, *22* (11), 1928.

Jaya, S., Durance, T., & Wang, R. (2009). Effect of alginate-pectin composition on drug release characteristics of microcapsules. *Journal of Microencapsulation*, *26* (2), 143-153.

Jayatissa, N. U., Unagolla, J., & Bhaduri, S. (2018). 3D PRINTED POLYMER SCAFFOLDS FOR BONE TISSUE ENGINEERING. *The Ohio Journal of Science*, *118* (1), A15-A16.

Juliano, C., Pala, C. L., & Cossu, M. (2007). Preparation and characterisation of polymeric films containing propolis. *Journal of Drug Delivery Science and Technology*, *17* (3), 177-182.

Kamoun, E. A., Kenawy, E.-R. S., Tamer, T. M., El-Meligy, M. A., & Eldin, M. S. M. (2015). Poly (vinyl alcohol)-alginate physically crosslinked hydrogel membranes for wound dressing applications: characterization and bio-evaluation. *Arabian Journal of Chemistry*, *8* (1), 38-47.

Kedzia, B., & Holderna-Kedzia, E. (2013). Aktywność antybiotyczna propolisu krajowego i europejskiego. *Postepy Fitoterapii*, *2* , 97-107.

Keskin, M., Keskin, Ş., & Kolayli, S. (2019). Preparation of alcohol free propolis-alginate microcapsules, characterization and release property. *LWT*, *108* , 89-96.

Kogelenberg, S. v., Yue, Z., Dinoro, J. N., Baker, C. S., & Wallace, G. G. (2018). Three-dimensional printing and cell therapy for wound repair. *Advances in wound care*, *7* (5), 145-156.

- Konta, A. A., García-Piña, M., & Serrano, D. R. (2017). Personalised 3D printed medicines: which techniques and polymers are more successful? *Bioengineering*, 4 (4), 79.
- Kujumgiev, A., Tsvetkova, I., Serkedjieva, Y., Bankova, V., Christov, R., & Popov, S. (1999). Antibacterial, antifungal and antiviral activity of propolis of different geographic origin. *Journal of ethnopharmacology*, 64 (3), 235-240.
- Lee, K. Y., & Mooney, D. J. (2012). Alginate: properties and biomedical applications. *Progress in polymer science*, 37 (1), 106-126.
- Liakos, I., Rizzello, L., Scurr, D. J., Pompa, P. P., Bayer, I. S., & Athanassiou, A. (2014). All-natural composite wound dressing films of essential oils encapsulated in sodium alginate with antimicrobial properties. *International journal of pharmaceutics*, 463 (2), 137-145.
- Liaw, C.-Y., & Guvendiren, M. (2017). Current and emerging applications of 3D printing in medicine. *Biofabrication*, 9 (2), 024102.
- Lu, H., Oh, H. H., Kawazoe, N., Yamagishi, K., & Chen, G. (2012). PLLA–collagen and PLLA–gelatin hybrid scaffolds with funnel-like porous structure for skin tissue engineering. *Science and technology of advanced materials*, 13 (6), 064210.
- Luo, Y., Luo, G., Gelinsky, M., Huang, P., & Ruan, C. (2017). 3D bioprinting scaffold using alginate/polyvinyl alcohol bioinks. *Materials Letters*, 189 , 295-298.
- M. C. Straccia, I. R., A. Oliva, G. Santagata and P. Laurienzo. (2014). *Carbohydrate Polymers* (Vol. 108).
- Maji, K., Dasgupta, S., Pramanik, K., & Bissoyi, A. (2016). Preparation and evaluation of gelatin-chitosan-nanobioglass 3D porous scaffold for bone tissue engineering. *International journal of biomaterials*, 2016 .
- Martín-Ramos, P., Fernández-Coppel, I. A., Ruíz-Potosme, N. M., Martín-Gil, J., Martín-Ramos, P., Fernández, I., & Miguel, N. (2018). Potential of ATR-FTIR spectroscopy for the classification of natural resins. *BEMS Rep*, 4 (1), 03-06.
- Martinotti, S., & Ranzato, E. (2015). Propolis: a new frontier for wound healing? *Burns & Trauma*, 3 (1), 9.
- Mimmo, T., Marzadori, C., Montecchio, D., & Gessa, C. (2005). Characterisation of Ca- and Al-pectate gels by thermal analysis and FT-IR spectroscopy. *Carbohydrate Research*, 340 (16), 2510-2519.
- Mouhoubi-Tafnine, Z., Ouchemoukh, S., & Tamendjari, A. (2016). Antioxydant activity of some algerian honey and propolis. *Industrial Crops and Products*, 88 , 85-90.
- Moura, S. A. L. d., Negri, G., Salatino, A., Lima, L. D. d. C., Dourado, L. P. A., Mendes, J. B., . . . Cara, D. C. (2011). Aqueous extract of Brazilian green propolis: primary components, evaluation of inflammation and wound healing by using subcutaneous implanted sponges. *Evidence-Based Complementary and Alternative Medicine*, 2011 .
- Naseri, N., Poirier, J.-M., Girandon, L., Fröhlich, M., Oksman, K., & Mathew, A. P. (2016). 3-Dimensional porous nanocomposite scaffolds based on cellulose nanofibers for cartilage tissue engineering: tailoring of porosity and mechanical performance. *Rsc Advances*, 6 (8), 5999-6007.
- Ngo, T. D., Kashani, A., Imbalzano, G., Nguyen, K. T., & Hui, D. (2018). Additive manufacturing (3D printing): A review of materials, methods, applications and challenges. *Composites Part B: Engineering*, 143 , 172-196.
- Nina, N., Lima, B., Feresin, G. E., Giménez, A., Salamanca Capusiri, E., & Schmeda-Hirschmann, G. (2016). Antibacterial and leishmanicidal activity of Bolivian propolis. *Letters in applied microbiology*, 62 (3), 290-296.

Odellius, K., Hoglund, A., Kumar, S., Hakkarainen, M., Ghosh, A. K., Bhatnagar, N., & Albertsson, A.-C. (2011). Porosity and pore size regulate the degradation product profile of polylactide. *Biomacromolecules*, *12* (4), 1250-1258.

Oh, S. H., Park, I. K., Kim, J. M., & Lee, J. H. (2007). In vitro and in vivo characteristics of PCL scaffolds with pore size gradient fabricated by a centrifugation method. *Biomaterials*, *28* (9), 1664-1671.

Oliveira, A. V., Ferreira, A. L., Nunes, S., Dandlen, S. A., Miguel, M. d. G., & Faleiro, M. L. (2017). Antibacterial activity of propolis extracts from the south of Portugal. *Pakistan journal of pharmaceutical sciences*, *30* (1).

Oliveira, R. N., Mancini, M. C., Oliveira, F. C. S. d., Passos, T. M., Quilty, B., Thiré, R. M. d. S. M., & McGuinness, G. B. (2016). FTIR analysis and quantification of phenols and flavonoids of five commercially available plants extracts used in wound healing. *Matéria (Rio de Janeiro)*, *21* (3), 767-779.

Oliveira, R. N., McGuinness, G. B., Ramos, M. E. T., Kajiyama, C. E., & Thiré, R. M. (2016). *Properties of PVA Hydrogel Wound-Care Dressings Containing UK Propolis*. Paper presented at the Macromolecular Symposia.

Oliveira, R. N., McGuinness, G. B., Rouze, R., Quilty, B., Cahill, P., Soares, G. D., & Thire, R. M. (2015). PVA hydrogels loaded with a Brazilian propolis for burn wound healing applications. *Journal of Applied Polymer Science*, *132* (25).

Oliveira, R. N., Moreira, A. P. D., Thire, R. M. d. S. M., Quilty, B., Passos, T. M., Simon, P., . . . McGuinness, G. B. (2017). Absorbent polyvinyl alcohol-sodium carboxymethyl cellulose hydrogels for propolis delivery in wound healing applications. *Polymer Engineering & Science*, *57* (11), 1224-1233.

Oryan, A., Alemzadeh, E., & Moshiri, A. (2018). Potential role of propolis in wound healing: Biological properties and therapeutic activities. *Biomedicine & Pharmacotherapy*, *98* , 469-483.

Ouyang, L., Yao, R., Zhao, Y., & Sun, W. (2016). Effect of bioink properties on printability and cell viability for 3D bioplotting of embryonic stem cells. *Biofabrication*, *8* (3), 035020.

Pereira, R., Tojeira, A., Vaz, D. C., Mendes, A., & Bartolo, P. (2011). Preparation and characterization of films based on alginate and aloe vera. *International Journal of Polymer Analysis and Characterization*, *16* (7), 449-464.

Przybyłek, I., & Karpiński, T. M. (2019). Antibacterial Properties of Propolis. *Molecules (Basel, Switzerland)*, *24* (11), 2047. doi: 10.3390/molecules24112047

Salem, A. K., Stevens, R., Pearson, R., Davies, M., Tendler, S., Roberts, C., . . . Shakesheff, K. (2002). Interactions of 3T3 fibroblasts and endothelial cells with defined pore features. *Journal of Biomedical Materials Research: An Official Journal of The Society for Biomaterials, The Japanese Society for Biomaterials, and The Australian Society for Biomaterials and the Korean Society for Biomaterials*, *61* (2), 212-217.

Serra, T., Mateos-Timoneda, M. A., Planell, J. A., & Navarro, M. (2013). 3D printed PLA-based scaffolds: a versatile tool in regenerative medicine. *Organogenesis*, *9* (4), 239-244.

Sforcin, J. M. (2016). Biological properties and therapeutic applications of propolis. *Phytotherapy research*, *30* (6), 894-905.

Sharaf, S., & El-Naggar, M. E. (2019). Wound dressing properties of cationized cotton fabric treated with carrageenan/cyclodextrin hydrogel loaded with honey bee propolis extract. *International journal of biological macromolecules*, *133* , 583-591.

Silici, S., & Kutluca, S. (2005). Chemical composition and antibacterial activity of propolis collected by three different races of honeybees in the same region. *Journal of ethnopharmacology*, *99* (1), 69-73.

- Silva, R. P. D., Machado, B. A. S., de Abreu Barreto, G., Costa, S. S., Andrade, L. N., Amaral, R. G., . . . Umsza-Guez, M. A. (2017). Antioxidant, antimicrobial, antiparasitic, and cytotoxic properties of various Brazilian propolis extracts. *Plos one*, *12* (3), e0172585.
- Simpson, N. E., Stabler, C. L., Simpson, C. P., Sambanis, A., & Constantinidis, I. (2004). The role of the CaCl₂-gulosonic acid interaction on alginate encapsulated β TTC3 cells. *Biomaterials*, *25* (13), 2603-2610.
- Stangl, R., Rinne, B., Kastl, S., & Hendrich, C. (2001). The influence of pore geometry in cp Ti-implants—A cell culture investigation. *Eur Cell Mater*, *2* (2), 1-9.
- Straccia, M., d'Ayala, G., Romano, I., Oliva, A., & Laurienzo, P. (2015). Alginate hydrogels coated with chitosan for wound dressing. *Marine drugs*, *13* (5), 2890-2908.
- Sultan, S., & Mathew, A. P. (2018). 3D printed scaffolds with gradient porosity based on a cellulose nanocrystal hydrogel. *Nanoscale*, *10* (9), 4421-4431.
- Sutjarittangtham, K., Sanpa, S., Tunkasiri, T., Rachtanapun, P., Chantawannakul, P., Intatha, U., . . . Eitssayeam, S. (2012). *Preparation of polycaprolactone/ethanolic extract propolis nanofibers films*. Paper presented at the Advanced Materials Research.
- Torre, M. L., Giunchedi, P., Maggi, L., Steffi, R., Machiste, E. O., & Conte, U. (1998). Formulation and characterization of calcium alginate beads containing ampicillin. *Pharmaceutical development and technology*, *3* (2), 193-198.
- Uzun, M., Anand, S., & Shah, T. (2012). The effect of wound dressings on the pH stability of fluids. *Journal of wound care*, *21* (2), 88-95.
- Valenzuela-Barra, G., Castro, C., Figueroa, C., Barriga, A., Silva, X., de las Heras, B., . . . Delporte, C. (2015). Anti-inflammatory activity and phenolic profile of propolis from two locations in Región Metropolitana de Santiago, Chile. *Journal of ethnopharmacology*, *168* , 37-44.
- Vieira, T., Silva, J. C., do Rego, A. B., Borges, J. P., & Henriques, C. (2019). Electrospun biodegradable chitosan based-poly (urethane urea) scaffolds for soft tissue engineering. *Materials Science and Engineering: C* , 109819.
- Yang, F., Zhang, M., Bhandari, B., & Liu, Y. (2018). Investigation on lemon juice gel as food material for 3D printing and optimization of printing parameters. *LWT*, *87* , 67-76.
- Yannas, I., Lee, E., Orgill, D. P., Skrabut, E., & Murphy, G. F. (1989). Synthesis and characterization of a model extracellular matrix that induces partial regeneration of adult mammalian skin. *Proceedings of the National Academy of Sciences*, *86* (3), 933-937.
- Yildirim, A., Duran, G. G., Duran, N., Jenedi, K., Bolgul, B. S., Miraloglu, M., & Muz, M. (2016). Antiviral activity of hatay propolis against replication of herpes simplex virus type 1 and type 2. *Medical science monitor: international medical journal of experimental and clinical research*, *22* , 422.
- You, F., Wu, X., & Chen, X. (2017). 3D printing of porous alginate/gelatin hydrogel scaffolds and their mechanical property characterization. *International Journal of Polymeric Materials and Polymeric Biomaterials*, *66* (6), 299-306.
- Zardiackas, L. D., Parsell, D. E., Dillon, L. D., Mitchell, D. W., Nunnery, L. A., & Poggie, R. (2001). Structure, metallurgy, and mechanical properties of a porous tantalum foam. *Journal of Biomedical Materials Research: An Official Journal of The Society for Biomaterials, The Japanese Society for Biomaterials, and The Australian Society for Biomaterials and the Korean Society for Biomaterials*, *58* (2), 180-187.
- Zhang, H., Fu, Y., Niu, F., Li, Z., Ba, C., Jin, B., . . . Li, X. (2018). Enhanced antioxidant activity and in vitro release of propolis by acid-induced aggregation using heat-denatured zein and carboxymethyl chitosan. *Food hydrocolloids*, *81* , 104-112.

Zhang, H., Zhou, L., & Zhang, W. (2014). Control of scaffold degradation in tissue engineering: a review. *Tissue Engineering Part B: Reviews*, 20 (5), 492-502.

Zheng, J., Yu, X., Wang, C., Cao, Z., Yang, H., Ma, D., & Xu, X. (2016). Facile synthesis of three-dimensional reinforced Sn@ polyaniline/sodium alginate nanofiber hydrogel network for high performance lithium-ion battery. *Journal of Materials Science: Materials in Electronics*, 27 (5), 4457-4464.

Samples	Viscosity (mPa.s)	Density (kg/m ³)	Surface Tension (mN.m ⁻¹)	Image of 20 layer printed scaffold
Sample 1	6109	1.022 ± 0.02	39.43	
Sample 2	8018	1.023 ± 0.03	44.73	
Sample 3	8028	1.024 ± 0.02	64.78	
Sample 4	Measurement failed	Measurement failed	Measurement failed	

Table 1: Physical properties summarize of scaffolds

Table 2: Fitting Experimental Release Data, from the Ps release of 3D printed scaffolds to Higuchi and Korsmeyer-Peppas Kinetic Equations for neutral and acidic conditions (pH 7.4 and 2)

	Higuchi	Higuchi	Higuchi	Korsmeyer-Peppas	Korsmeyer-Peppas	Korsmeyer-Peppas
	R ²		K _h	R ²		n
pH 7.4	0.9822		6.025	0.9715		0.4492
pH 2.0	0.9515		7.9228	0.8633		0.6153

Table 3: Inhibition zone measurements of *S. aureus* and *E. coli* obtained with different Ps concentrations and ampicillin (2 and 10 µg).

	Inhibition zone (mm)				
Bacteria	SA ⁺	Ps ⁺⁺ low	Ps high	Ampicillin 2	Ampicillin 10
S.aureus	0	15,00±1,1	13,00±1,0	18,00±1,0	19,00±1,0
E.coli	0	0	0	NA	NA

+ SA, sodium alginate;

++ Ps, propolis

FIGURE LEGENDS

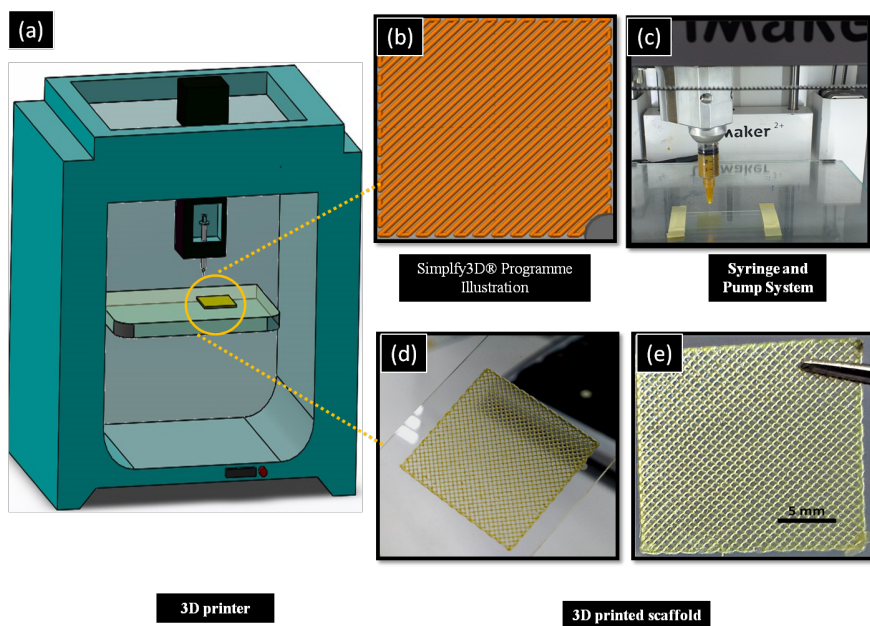


Figure 1: Schematic drawing of the experiment a) 3D printer b) Syringe pump system of machine c) Simplyf3D programme illustration of scaffolds d) 3D printed scaffold in glass slide before crosslinking e) After crosslinking of 3D printed scaffolds

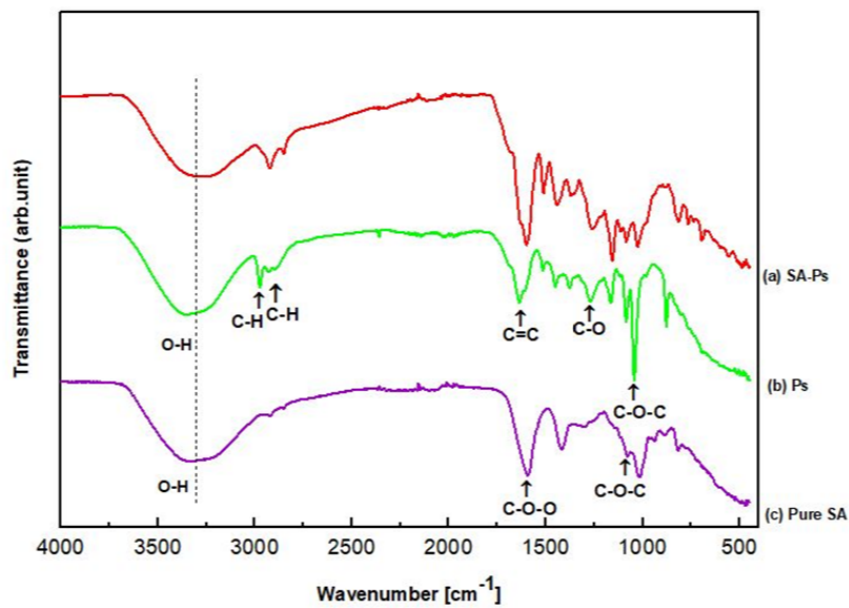


Figure 2: FT-IR spectrums of pure SA, Ps and SA with Ps

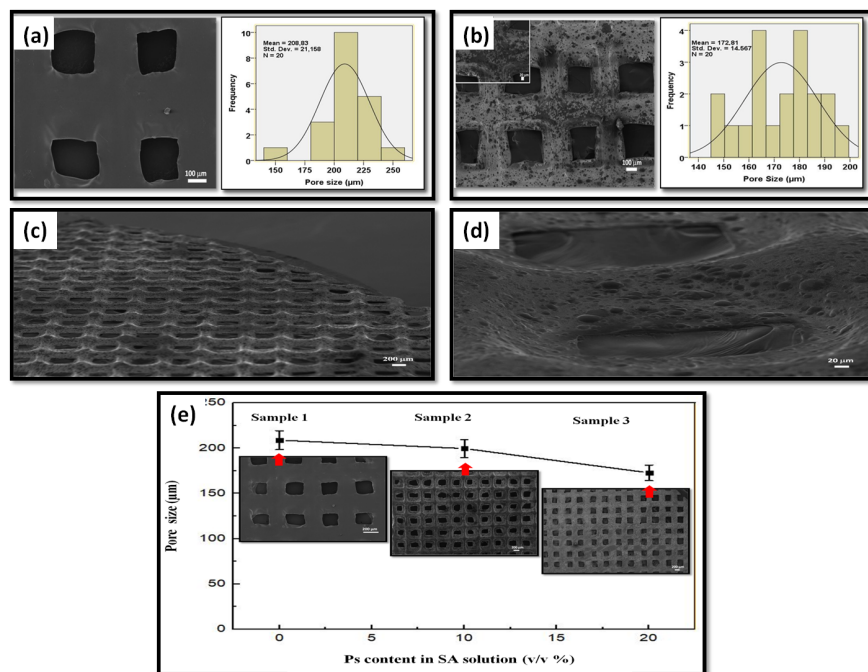


Figure 3: Sem images of 3D printed SA and Ps incorporated SA scaffolds (a) SA scaffolds and pore size histogram (Sample 1)(b) Ps incorporated SA scaffolds and pore size histogram (Sample 3) (c) SEM image of Ps – SA scaffold from different angle (d) Magnification of the scaffold pores (e) Pore size distribution according to propolis content

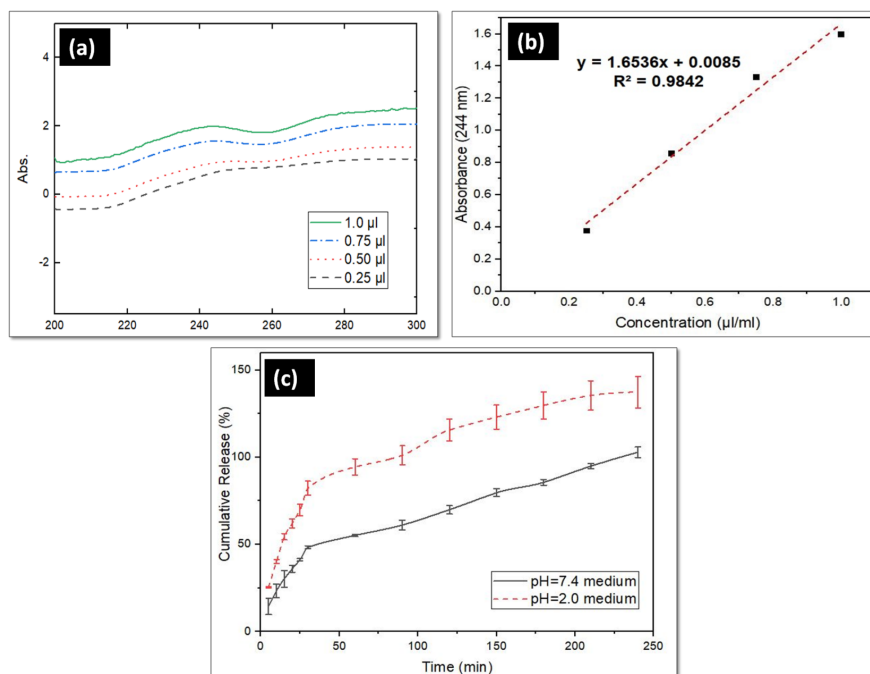


Figure 4: (a) Absorbance values according to different dilution ratios for the standard calibration curve

(b) Standard calibration curve of Ps solution (c) Release profile of 3D printed Ps incorporated SA scaffolds in different pH mediums

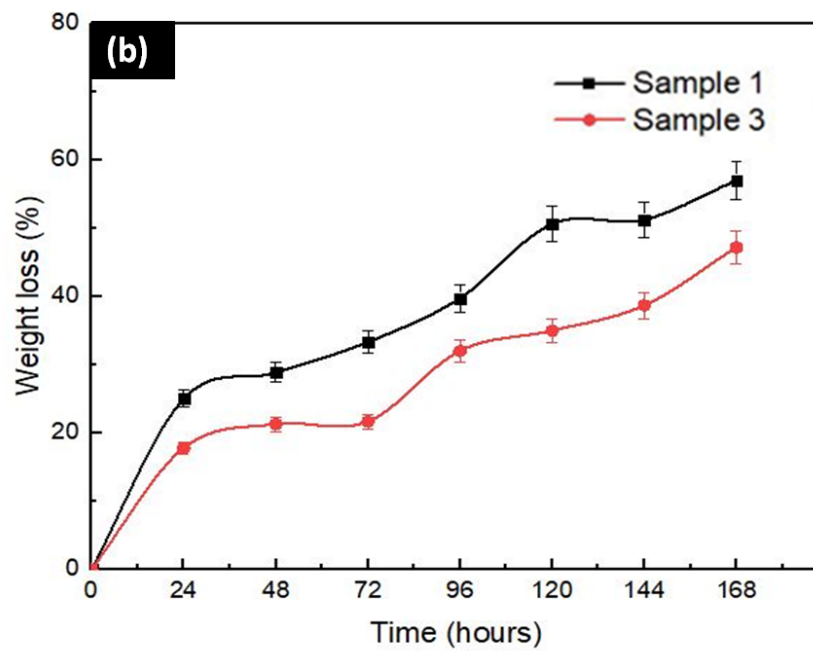
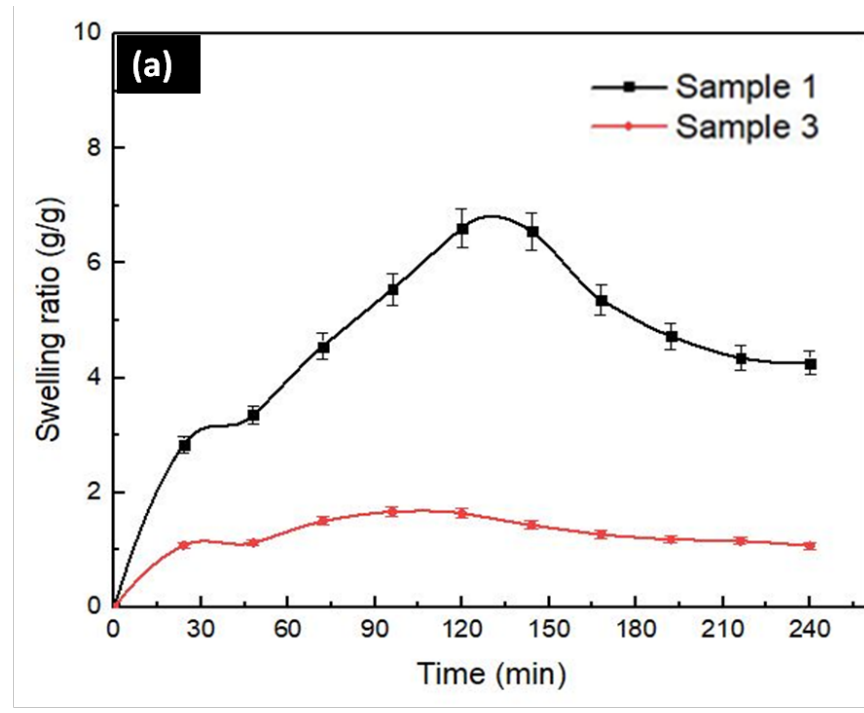


Figure 5: (a) Swelling and (b) Degradation kinetics of 3D printed Sample 1 and Sample 3 scaffolds in PBS 7.4 at 37°C

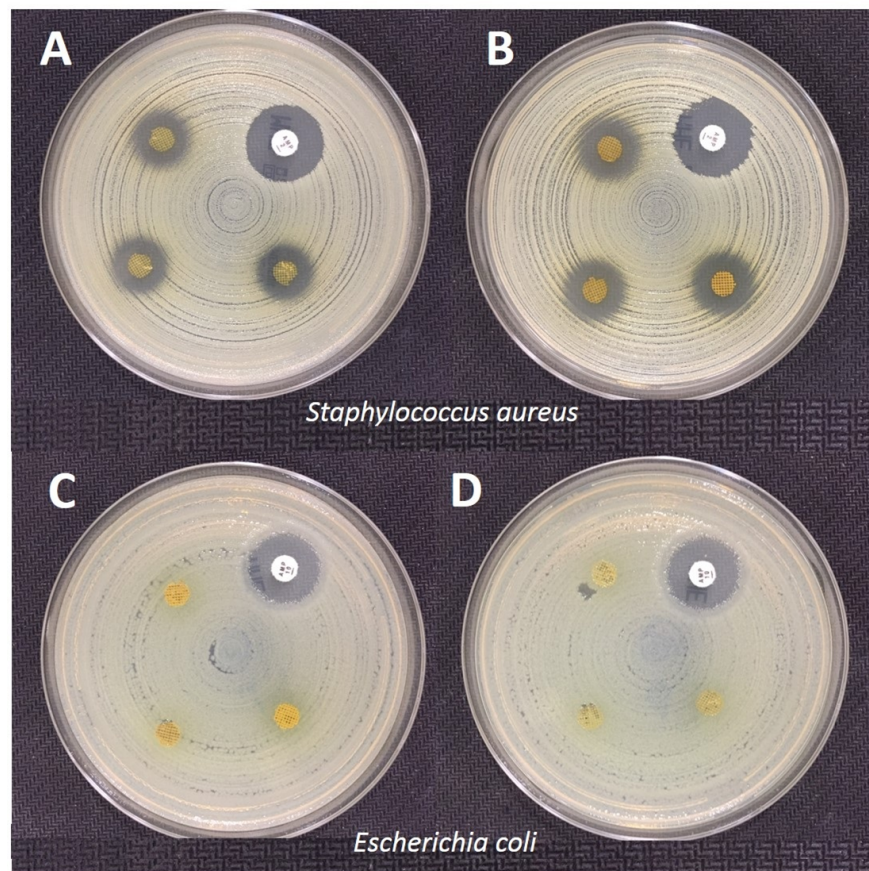


Figure 6: The inhibition zones of different Ps concentrations and ampicillin (2 and 10 μg) against *S. aureus* and *E. coli* after 18 h incubation at 37°C. A: Ampicillin 2 μg disk (1), Ps low concentration disks (2-4) with *S. aureus* ATCC® 29213; B: Ampicillin 2 μg disk (1), Ps high concentration disks (2-4) with *S. aureus* ATCC® 29213. C: Ampicillin 10 μg disk (1), Ps low concentration disks (2-4) with *E. coli* ATCC® 25922; D: Ampicillin 10 μg disk (1), Ps high concentration disks (2-4) with *E. coli* ATCC® 25922.

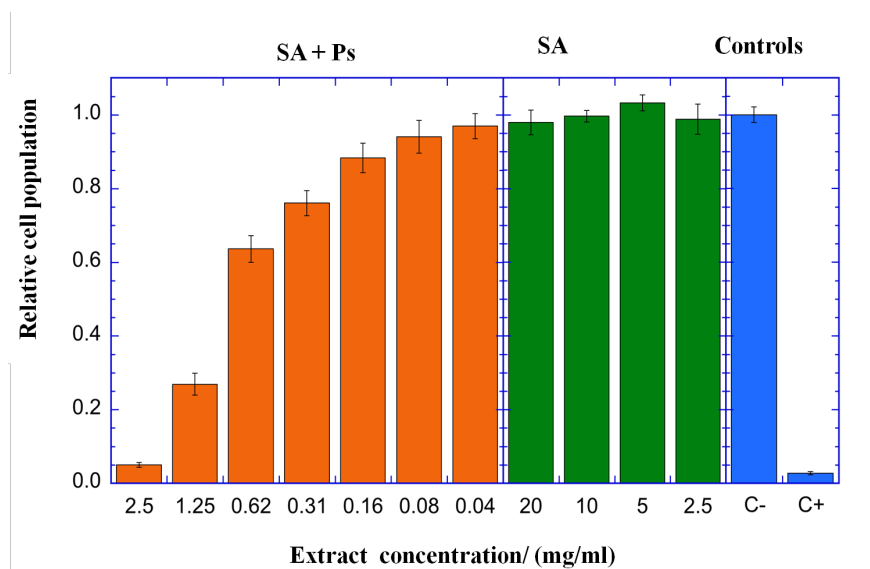


Figure 7: Results of the cytotoxicity test: cell populations calculated relative to the negative control show that extracts obtained with the SA scaffolds are non-cytotoxic for the concentrations tested and extracts obtained with the Ps containing scaffolds are severely cytotoxic for concentrations of 1.25 mg/ml and above but become non-cytotoxic at concentrations of 0.08 mg/ml and below.